Evidence for iceberg fertilization of the NW Atlantic

Grant R. Bigg[1], Quentin Jutard[2], Robert Marsh[3]

[1] Department of Geography, University of Sheffield, Sheffield S10 2TN, U. K.
[2] ENSTA ParisTech, 1024, Boulevard des Maréchaux, 91762 Palaiseau Cedex, France ; present address: Observatoire Océanologique de Villefranche S/Mer, Sorbonne Université, 4 place Jussieu, 75005 France
[3] School of Ocean and Earth Science, University of Southampton, European Way, Southampton SO14 3ZH, U. K.

Correspondence to: Grant R. Bigg (grant.bigg@sheffield.ac.uk)

Abstract. Icebergs are known to have a significant fertilizing impact on primary productivity in the Southern Ocean, but this link is yet to be investigated in the Northern Hemisphere. This study combines sightings of icebergs with satellite-derived ocean colour data from 1998 to 2015, to seek such a relationship in the NW Atlantic. Despite the obscuring coincidence of the seasonal iceberg flux with the spring bloom of chlorophyll, it is shown that there is a large-scale, one-month-lagged regional correlation between iceberg flux and chlorophyll levels. In addition, a spatial time-lag analysis is consistent with the main cause for the iceberg-chlorophyll relationship being through advection of the nutrients entrained in iceberg meltwater. This leads to a delayed fertilization response of 2-4 weeks. There are a range of possible sources for the nutrients likely leading to this delayed response. The Northern Hemisphere impact of iceberg meltwater on primary production is much less pronounced than in the Southern Ocean, but it is discernible.

1 Introduction

Icebergs in the Southern Ocean are known to encourage primary production around themselves through a combination of nutrient and trace element (e.g. iron) release in meltwater (Raiswell et al., 2008), as well as enhancing vertical mixing of nutrients through the ascent and entrainment of submarine meltwater plumes (Helly et al., 2011; Smith et al., 2013). Both satellite (Schwarz and Schodlok, 2009; Duprat et al., 2016; Wu and Hou, 2017) and observational (e.g. Smith et al., 2007; Helly et al., 2011; Biddle et al., 2015) studies have demonstrated this iceberg-driven ocean fertilization around Southern Ocean icebergs, with, in some cases, the impact being visible in plumes extending over several hundreds of kilometres from giant icebergs (Duprat et al., 2016). There are very few observations of the actual deep export of carbon arising from this process (Smith et al., 2011), and some controversy over the conversion of production to export in the Southern Ocean (Martin et al., 2013) and the relative contribution of iron from iceberg (Lancelot et al., 2009; Hopwood et al., 2019) or sediment (Wadley et al., 2014) sources to production. Nevertheless,

29   what limited Lagrangian sediment trap observations exist below typical iceberg depth (Smith et al., 2011) suggest

30   Antarctic icebergs may contribute some 10-20% of the net deep export of carbon across the Southern Ocean (Duprat et

31   al., 2016), and especially in the seasonal sea-ice zone (Wu and Hou, 2017).

32   In the Northern Hemisphere, many icebergs are calved from Greenland, among other sources (Bigg et al., 1997), every

33   year, with most icebergs that survive to exit their calving fjord entering the North Atlantic or adjacent waters. Many of

34   these eventually enter the Labrador Current (Smith et al., 2013). While the giant icebergs, with lengths exceeding 18

35   km, observed in the Southern Ocean almost never occur in the Northern Hemisphere, in some years well over a

36   thousand icebergs with lengths from 5 m up to 3-400 m remain in the Labrador Current as it passes the southern tip of

37   Newfoundland, at 48°N (Bigg et al., 2014). However, little is known of their impact on primary production in the North

38   Atlantic. Shulenburger (1983), while observing some evidence of nutrient mixing, found no evidence for enhanced

39   chlorophyll levels around a Greenland iceberg. Nevertheless, animals from higher trophic levels, such as fish

40   (Holmquist, 1958) and seabirds (Joiris, 2018), are found around Greenland icebergs, suggesting there is an enriched

41   ecosystem locally. In contrast to the iron limiting nature of the Southern Ocean, the Labrador Sea only becomes limited

42   in macronutrients (Harrison and Li, 2008) and micronutrients (Arrigo et al., 2017) in the summer. However, the high

43   latitude North Atlantic is seasonally iron-limited in the Irminger and Iceland Basins (Achterberg et al., 2018; Hopwood

44   et al., 2018). The upwelling meltwater plumes from the base of icebergs, which typically penetrate beneath the late

45   spring/summer mixed layer depth (see Yankovsky and Yashayaev (2014) for an example), potentially provide a means

46   of enhancing and prolonging the nutrient and iron levels in the vicinity of the icebergs. Meltwater from the icebergs

47   themselves, however, also provides a potential means of widespread distribution of iron and nutrients from the

48   Greenland ice sheet, because open ocean iceberg delivery bypasses removal processes in fjords (Hopwood et al., 2019),

49   estuaries and coastal regions (in marked contrast to meltwater or riverine fluxes). In this context it is worth noting that

50   bio-available iron is potentially glacially preserved, and increased through utraviolet light reactions within ice with

51   near-surface sediment (Raiswell et al., 2018), and would then survive until release by melting.

52   The iceberg flux in the Labrador Current typically peaks in April (Bigg et al., 2014), coinciding with the onset of the

53   spring phytoplankton bloom (Fig. 1) – a co-occurrence to which we will return later. However, in the spring of the year

54   with the highest observed iceberg numbers crossing the 48°N parallel (2014; > 1500) since the MODIS ocean colour

55   satellite instruments became available in 2003, while there is a suggestion of enhanced production relative to the long-

56   term mean (area average of 0.79 mg m^{-3}), low iceberg years (e.g. 2006 with none and 2010 with 1) had similar or higher

57   average spring production (Fig. 1). There is thus a complex relationship between annual spring productivity over the

58   NW Atlantic and environmental variability, of which the iceberg flux is only a part. Other, largely independent, factors

59   which will affect the strength and timing of the spring bloom will be the intensity and depth of the previous winter's

60   ocean mixing, the rate of spring stratification, and the strength and timing of spring snow-fed river runoff through the

61   St. Lawrence River system. These will all be linked to recent past seasonal weather variability. Therefore, this paper

62   will attempt to control for these other climate factors by exploring more detailed statistical comparisons of both

63   temporal and spatial relationships between iceberg numbers and chlorophyll levels in the NW Atlantic. The aim is thus

64   to address the productivity component of the question raised by Smith et al. (2013): "Do icebergs in the Arctic also

65   exhibit enrichment or alteration processes of the pelagic ecosystem, ultimately leading to enhanced productivity and

66   carbon export?"

67
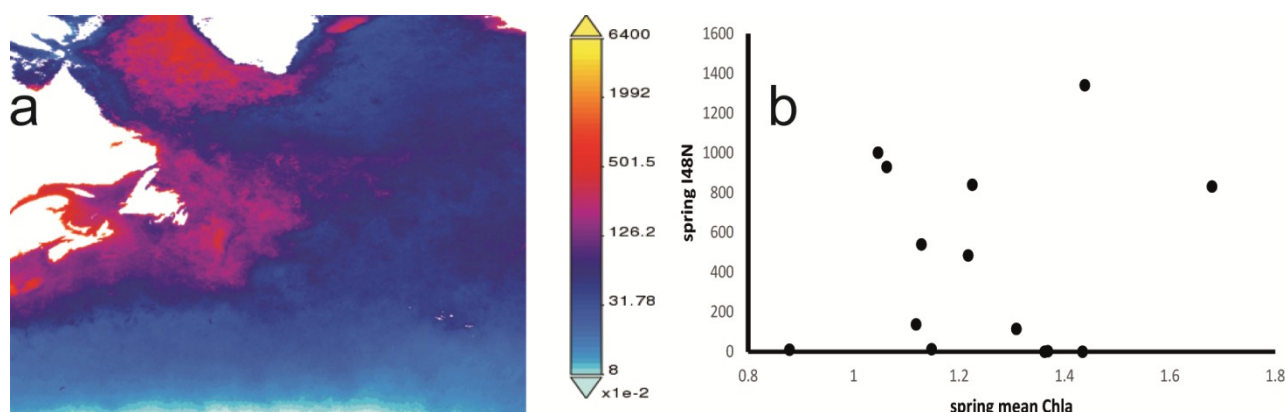
68   **Figure 1: Mean March-May surface chlorophyll levels (in mg m^{-3}; note logarithmic scale) from the 8-daily 4 km**

69   **MODIS ocean colour instrument over the NW Atlantic for 2003-2016: a) spatial pattern of mean, b) scatter plot**

70   **of spring mean chlorophyll a (chla) vs. spring I48N total. The visualization in a, and the data contributing to b**

71   **were produced within the GIOVANNI online data system, developed and maintained by the NASA GES DISC.**

72

73   **2 Data and Methods**

74   Two main types of data are used in this analysis: iceberg sightings and remotely sensed ocean colour, the latter being a

75   proxy for surface chlorophyll a concentration. There is a record of monthly iceberg numbers crossing the 48°N parallel

76   extending back to 1900 (Bigg et al., 2014), and daily iceberg sighting maps back to 2004 for regions south of 52°N. In

77   addition, a more complete database of iceberg sightings in the Labrador Sea exists from 1960 (IIP, 2016). This does not

78   have all size and shape fields specified for each sighting, varies in format over time, and certainly earlier data has some

79   quality control issues (Wilton et al., 2015). However, the location and timing of all iceberg sightings south of 52°N is

80   available for several decades. Ocean colour data is available in a fairly regular form only since the SeaWiFS satellite

81   was launched in 1998, but to obtain a full time series since then requires merging of data from more than one

82   instrument, thus requiring calibration. The next section therefore addresses how consistent datasets over our baseline

83   period of 1998-2015 were created from disparate sources.

84

2.1 Data

2.1.1 Ocean Colour

The chlorophyll data were retrieved from https://oceancolor.gsfc.nasa.gov/ for the two satellites SeaWiFS and MODIS-Aqua for the periods 1998-2002 and 2003-2015 respectively. The following 4 km resolution, Level 3 processed data were collected and averaged over a 1^ox1^o grid: a) monthly averages; b) 8 day averages that included the 15th of each month (not always over the same days of the month) to give a mid-month series; c) the 8 day averages that followed those from b); and d) daily averages that were used to calculate 2-7 day averages over the whole year. Note that the mean chlorophyll levels from these two satellites differ, and this difference has some spatial variability (Djavidnia et al., 2010), with the SeaWiFS chlorophyll typically being lower than the MODIS-Aqua values, with a weaker seasonal cycle. It was therefore decided to standardise the entire dataset so that the SeaWiFS and MODIS periods had the same mean and variance, using

$$S = \bar{M} + \frac{\sigma(M)}{\sigma(S)}(S - \bar{S}),$$ (1)

where S and M are the time series of SeaWiFS and MODIS data respectively, σ is the relevant standard deviation of the whole series and the overbar represents the respective series mean. The impact of this is shown in Supplementary Fig. S1.

2.1.2 Iceberg data

Two types of iceberg data were used in this study. As a measure of the overall flux of icebergs in the Labrador Current monthly estimates of the number of icebergs crossing 48^oN are compiled by the International Ice Patrol (IIP); here we define this as I48N. These data are available from 1900 to 2020 (http://www.navcen.uscg.gov/pdf/iip/International_Ice_Patrols_Iceberg_Counts_1900_to_2011.pdf , supplemented by subsequent annual reports available at https://www.navcen.uscg.gov/?pageName=IIPAnnualReports), although this study only uses the 1998-2015 period for analyses involving I48N, for consistency with the individual sightings database discussed below. A full discussion of the creation and quality of this dataset is given by Christensen and Luzader (2012) and Wilton et al. (2015). It is sufficient here to say that over the time period considered in this research a uniform approach to compiling the monthly count was employed, using a combination of dedicated aircraft surveys, ship reports, short-term iceberg drift modelling and some remote sensing input. Reference to any recent annual report will show the care taken by the IIP in compiling an accurate record, because of the importance of knowing the location of every iceberg threat to safe navigation.

113   The second type of iceberg data is the location of individual icebergs over the Labrador Sea. The form of this spatio-

114   temporal data varies over time. Over 2009-2015, iceberg positions for the 15th of each month were gridded from the

115   appropriate daily IIP iceberg chart (https://www.navcen.uscg.gov/?pageName=iipCharts), to a 1 degree precision. To

116   extend the record back to 1998, to coincide with the beginning of the SeaWiFS observation period, we used the IIP

117   iceberg sightings database (IIP, 2016). The observations in this database, which often only contain position and no size

118   information, are predominantly south of 52°N so the area over which the iceberg number density was calculated for this

119   study was limited to being south of 52°N. This region, from 52°N to the most southerly iceberg measurement and from

120   the eastern coast of North America out to the most easterly iceberg observation at 35°W, is defined as the main iceberg

121   area, or as region A. However, a technique needed to be designed to reconstruct the monthly map equivalent data from

122   this sightings database over the 1998-2008 period, when iceberg location maps were not available.

123   The period from 2009-2015 was used to test techniques for reconstructing number density fields in region A in the pre-

124   2009 period, as the daily charts changed format in 2009, with iceberg numbers becoming numerical rather than being

125   denoted by symbols from that year. The iceberg density reconstruction technique selected used the fact that trajectories

126   of individually identified icebergs in the sightings database could be calculated. This enabled the generation of a

127   Markov chain describing the probability that, after successive days, an iceberg would travel from a given grid square to

128   another. Markov chains of varying temporal lengths can be evaluated, which enabled the determination of the shortest

129   period of prior information required to produce a statistically robust reconstruction for a particular day's iceberg

130   density. The procedure for creating an iceberg density map for the 15th of each month in this way is described in

131   Appendix A. This was the only day's density calculated each month, for compatibility with the 2009-2015 mid-month

132   data set, described above. $I_{sightings}(x,y)$ is defined as the number of icebergs at the grid point (x,y) as reconstructed from

133   applying the Markov chain.

134   Measures of the number of icebergs found from the mapping database, $N_{maps}(x,y,n)$, and the sightings database,

135    $N_{sightings}(x,y,n)$, respectively are then defined. Here n is the size of area being compared and varies over squares of size

136   1°, 3°, 5° or 7°. Thus

137    $$N_{maps}(x, y, n) = \frac{1}{n^2}\sum_{(i,j)=-\frac{n-1}{2}}^{\frac{n-1}{2}} I_{maps}(x + i, y + j) \tag{2}$$

138   and

139    $$N_{sightings}(x, y, n) = \frac{1}{n^2}\sum_{(i,j)=-\frac{n-1}{2}}^{\frac{n-1}{2}} I_{sightings}(x + i, y + j) \tag{3}$$

140   with (x,y) being (longitude, latitude) of each respective square, $I_{maps}(x,y)$ being the number of icebergs at the grid point

141   (x,y) on the IIP maps and $I_{sightings}(x,y)$ deriving from the iceberg sightings database as described above.

142   A measure of the fit of the monthly map reconstruction using the sightings database is the correlation coefficient C_n,

143   where C_n is given by:

144 $$C_n = \frac{\sum_{(x,y)\in A} N_{maps}(x,y,n) N_{sightings}(x,y,n)}{\sqrt{\sum_{(x,y)\in A}(N_{maps}(x,y,n))^2 \sum_{(x,y)\in A}(N_{sightings}(x,y,n))^2}}.$$ (4)

145 The overall correlation of the method to be discussed below can then be expressed in an iceberg number weighted

146 mean, $C_{T,n}$, over the 84 months from January 2009 to December 2015, where

147 $$C_{T,n} = \frac{\sum_{m=1}^{84} C_n (\sum_{(x,y)\in A} I_{maps}(x,y,n))}{\sum_{m=1}^{84} \sum_{(x,y)\in A} I_{maps}(x,y,n)}.$$ (5)

148 The correlation measure $C_{T,n}$ is shown in Fig. 2. Here the dependence of $C_{T,n}$ on the length of time before the selected

149 day over which the Markov chain is constructed is shown. Even for the finest resolution of 1 degree squares, $C_{T,1}$

150 reaches ~ 0.7 if 16 or more previous days are used, while for the bigger squares $C_{T,n}$ exceeds 0.95 for those cases. Later

151 analysis in this paper covers the period 1998-2015, where the iceberg density fields for 1998-2008 are reconstructed

152 using a Markov chain extending over 16 days prior to the nominal 15th of each month, and are combined with the mid-

153 month map iceberg density record used for 2009-2015.

154
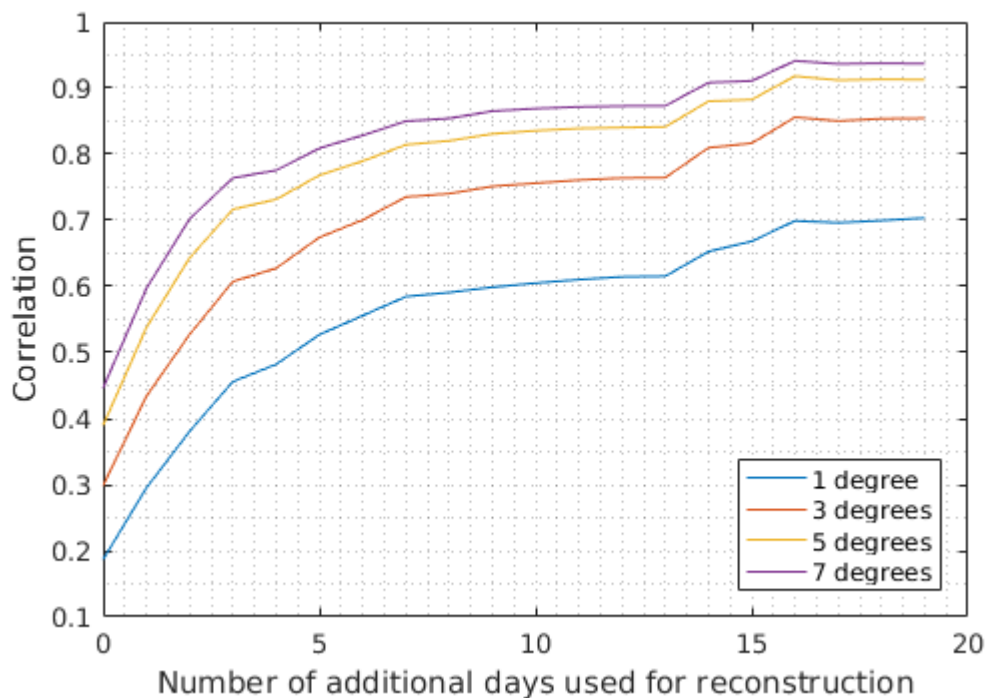
155 **Figure 2: The overall correlation, $C_{T,n}$, for n=1, 3, 5 and 7 degree squares for reconstructing the observed data**

156 **over 2009-2015 using the Markov chain approach.**

157

2.2 Methods

158

159 Seeking an unequivocal link between iceberg fluxes and chlorophyll levels in the Labrador Sea is complicated by the

160 temporal correspondence of the peak iceberg season of spring and early summer with the marine productivity spring

161 bloom (Zhao et al., 2013), in a region close to coasts, with rivers which will have major seasonal variability, including a

162 spring peak flow due to snow melt (Vorosmarty et al., 1998), and considerable benthic sediment resuspension from

163 extensive shallow shelves. The latter can be of similar magnitude to fluxes of iceberg iron (Wadley et al., 2014;

164 Raiswell et al., 2016). Remote sensing analysis in the Southern Ocean also suggests that the impact of fertilization from

165 melting icebergs can have a time lag of some weeks (Schwarz and Schodlock, 2009; Duprat et al., 2016). Two methods,

166 using different mixtures of iceberg and chlorophyll datasets, were employed to try to disentangle any signal from what

167 will be a complex and multiply-forced environment. This task is made even more complicated by the sub-grid scale size

168 of icebergs in the Labrador Sea, relative to ocean colour pixels, compared to the often much larger Southern Ocean

169 icebergs. The two basic methods are described here, with the results of the relevant analyses given in the Results

170 section.

2.2.1 Large-scale comparison

172 The first approach to seek a link between iceberg flux and chlorophyll levels uses large-scale comparisons between the

173 IIP's monthly iceberg number crossing 48°N (I48N), and a monthly average chlorophyll over the main area of the

174 Labrador Sea through which icebergs drift, or where meltwater entrained in the North Atlantic Drift may be advected

175 over later weeks. A nearby coastal area, which will experience many of the same environmental forcings as the main

176 area, but which almost no icebergs reach, and little iceberg meltwater (see Fig. 13 of Wilton et al., 2015), was also

177 defined as a control area. The main area, or region A, and a control area are shown in Fig. 3.
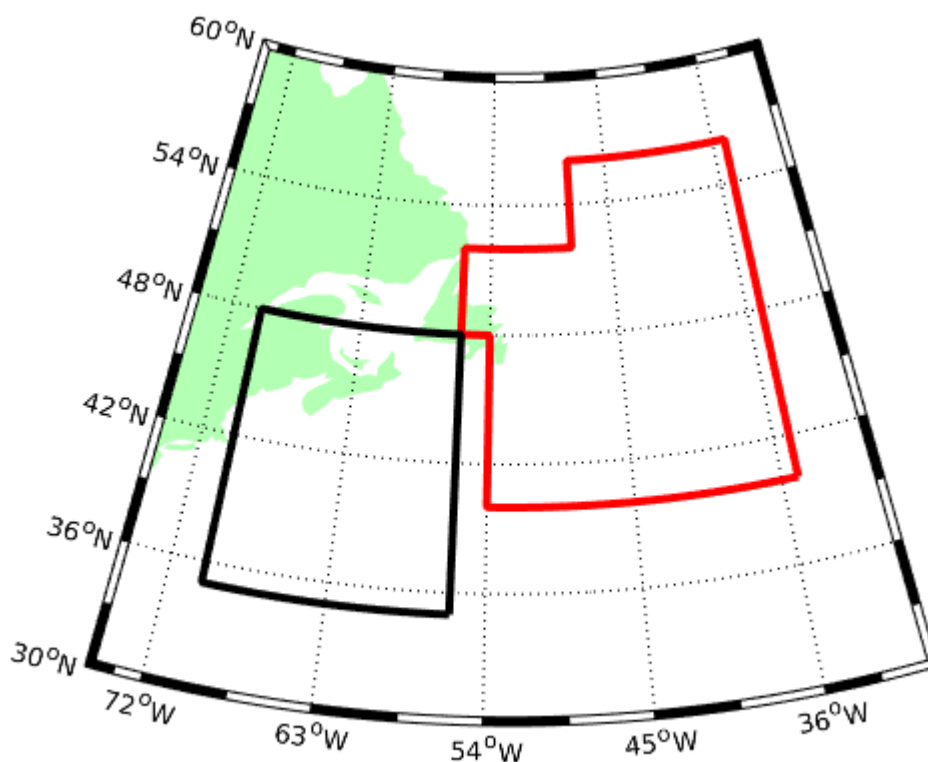
Figure 3: Definition of the main iceberg area (area A, in red) and the control area (black).

To confirm that the control area productivity is indeed experiencing similar environmental forcings to those in the iceberg main area, a series of correlation tests of the MODIS chlorophyll data between the control and iceberg main areas were carried out. Over the almost 18 year period of July 2002 – May 2020 the monthly mean chlorophyll in the control region, at 0.56 ± 0.22 mg m^{-3}, is indistinguishable from that in the iceberg area (0.69 ± 0.19 mg m^{-3}), with a statistically significant correlation (at better than the 1% level) of 0.47. Note that this correlation increases to 0.61 if the impact of icebergs is minimized by correlating only months from the 5 years with less than 100 icebergs in total passing 48°N. That icebergs have an impact on the chlorophyll is seen by correlating the monthly mean chlorophyll between the control and iceberg areas for just the months during the peak iceberg season of April-June. Including all years leads to a statistically insignificant correlation of 0.12, while comparing this spring bloom period for years with less than 100 icebergs raises the correlation to 0.52, which is statistically significant at the 5% level. Thus, using chlorophyll in the control area as a means to control for the wider non-iceberg environmental factors affecting regional chlorophyll levels is a valid approach.

193   To do this, Pearson correlations were first calculated between the anomalies of the two parameters I48N and

194   chlorophyll (averaged over each of the control and main areas), relative to their monthly averages over the period 1998-

195   2015. These were calculated over a range of lags from -2 months to 2 months, where a lag > 0 means I48N leads the

196   chlorophyll. In addition, in order to attempt to correct for changes purely due to non-iceberg effects, partial correlations

197   (Stuart et al., 2008) using the monthly anomalies from the control area as a control parameter, were also carried out

198   using the Matlab function partialcorr (https://uk.mathworks.com/help/stats/partialcorr.html). This approach, of using

199   partial correlation analysis to control for common variation in processes unrelated to the main question being

200   investigated, has been successfully employed in a number of environmental fields, with recent examples in untangling

201   rain:aerosol relationships in marine remote sensing studies (Yang et al., 2016), whether carbon isotope fractionation in

202   phytoplankton is a proxy for pH (Wang et al., 2016) and the role of salmon species' density-dependence in growth

203   (Morita and Fukuwaka, 2020). The idea behind partial correlation is to minimize the impact of forcing processes

204   common to both variables (or regions in this case) on the resulting correlation. While partial correlation remains not the

205   same as causation, a significant partial correlation increases confidence that there may be a plausible link between the

206   two correlating variables.

207   **2.2.2 Local temporal comparison**

208   A more local approach was to carry out a temporally lagged correlation the total of the mid-monthly icebergs recorded

209   over the main area (Fig. 3), I_T, obtained from the spatial distribution constructed as described above in section 2.1.2,

210   with the time-lagged local chlorophyll across much of the North Atlantic (36-66°N, 75-30°W). It is worth noting that I_T

211   is used as the measure of iceberg number, rather than a spatial field, as the geographical distribution of icebergs is very

212   variable in both space and time and makes a completely local correlation problematic in all regions except near the

213   coast. In such areas the correlation is mostly statistically significant, but it is difficult to separate a direct iceberg effect

214   from the influence of other local environmental factors affecting chlorophyll levels. A large-scale measure of iceberg

215   number is therefore retained, but one with a contribution of much more spatial information than the IIP's I48N

216   employed in the last section.

217   The correlation was carried out over the full iceberg season (February to August; Bigg et al. (2014)). As with the large-

218   scale comparison method described in the last section, the data used were monthly anomalies. To minimize the impact

219   of natural variability in the chlorophyll field linked directly or indirectly across the whole North Atlantic to variability

220   in the weather a control parameter was also used here to produce a partial correlation. This control parameter needed to

221   have a more extensive spatial and physical remit than the control area chlorophyll used in the last section, while still

222   being largely independent of the iceberg measure, I_T. After a range of tests, the control parameter was chosen to be the

223   North Atlantic Oscillation (NAO), using the NAO Index of Hurrell and Deser (2009;

224   https://climatedataguide.ucar.edu/climate-data/hurrell-north-atlantic-oscillation-nao-index-pc-based). The NAO is a

225 large scale measure of the tropospheric circulation over the North Atlantic, strongly linked to Arctic atmospheric

226 circulation as well as being highly correlated with a range of climatic factors across the northern Atlantic (Hurrell and

227 Deser, 2009; Reintges et al., 2017). However, previous work has shown that the NAO is not linearly correlated with the

228 Greenland Ice Sheet mass balance (Hanna et al., 2011), which is one of the main variables indirectly responsible for the

229 Greenland iceberg flux (Zhao et al., 2016). There is a weak, non-linear, link between significantly lagged (> 6 months)

230 NAO and I48N (Zhao et al., 2016), nevertheless, the recent NAO Index can be used as a control parameter as it affects

231 current and recent climate, but not iceberg flux.

232 The control parameter uses the NAO lagged by 3 months compared to the month of examination, as this lag had the

233 most impact on reducing the natural variability component of the chlorophyll. Note that the use of partial correlation

234 analysis as a way to remove the impact of specific climate signals from a process study is common, with recent

235 examples in untangling rainfall/cyclone:sea temperature relationships (He et al., 2016; Hong et al., 2018; Srinivas et al.,

236 2018), and the impact of the lower stratosphere on tropical cyclone intensity (Ferrara et al., 2017).

237 As Southern Ocean analyses have shown that the time lag between iceberg melting and ocean fertilization is likely to be

238 days to weeks (Schwartz and Schodlok, 2009; Duprat et al., 2016), the daily chlorophyll data at each point across the

239 North Atlantic were converted into a series of 5 day average fields. The measures I_T and the NAO Index, were then

240 linearly interpolated between their monthly values to provide analogous 5-day series over 1998-2015, 5 day averages

241 being chosen to reduce the impact of cloud cover on chlorophyll observations. Restricting the analysis to the peak

242 iceberg months of February-August, and using a control parameter of the 3-month lagged NAO Index, I_T and the

243 chlorophyll field were then partially correlated over a set of 5 day interval lags from 0 days to 70 days, with I_T leading.

244 This gives a measure of how any relationship between iceberg number and chlorophyll not dependent on the NAO

245 spatially evolves over time across the NW Atlantic; the results of this analysis are shown below.

246

247 **3 Results**

248 **3.1 Large-scale comparison**

249 Fig. 4 shows the Pearson correlations between monthly anomalies of I48N and the monthly mean chlorophyll over both

250 the main area and the control region (Fig. 3), over the period 1998-2015. The methodology was described in section

251 2.2.1 above. Correlations with lags up to ± 2 months are shown, as well as partial correlations, controlling for the

252 chlorophyll levels in the control area. It is expected that correlations should be positive if there is any causal link and,

253 sensibly, only lags ≥ 0 months show any positive correlations. However, the only correlations of any sign statistically

254 significant at the 0.05 level (correlations > |0.131|, 212 degrees of freedom) are those with a 1 month lag. Here, the

255 correlation of I48N with the main area chlorophyll is significant, and this is also true in the partial correlation case,

256 when controlled for the chlorophyll natural variability of the control area.

257
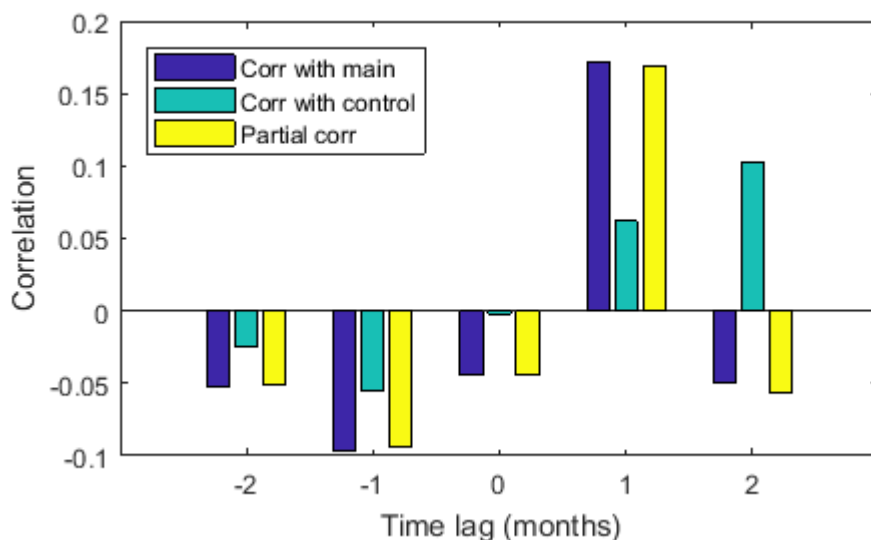
Figure 4: Lagged Pearson correlations between monthly chlorophyll anomalies in both main and control areas
and I48N, over 1998-2015. Only the +1 month correlation and partial correlation on the main area are
statistically significant at the 0.05% level (correlation coefficient > 0.134).

262   This result is consistent with there being a large-scale link between increasing iceberg numbers and fertilization of the

263   ocean a month later. It is suggestive rather than definitive, however, as the correlations are low in magnitude and the

264   increasing correlation of I48N with chlorophyll within the control area, with greater lag, is consistent with there being a

265   strong spring bloom amplification occurring after the peak iceberg flux of April/May. This result cannot shed light on

266   the question of the potential reality or cause of such a link, if real, whether it is restricted to the immediate vicinity of

267   the melting icebergs, extends to the mixing downstream of the iceberg meltwater with the ocean, or is a mixture of both

268   local and remote effects. In the next section we will explore this question further.

269   **3.2 Local temporally evolving comparison**

270   Fig. 5a shows a spatial view of the instantaneous correlation of monthly main area iceberg total number, I_T, with local

271   monthly mean chlorophyll, with the significant squares shown in Fig. 5b. This shows a region of zero-lag positive

272   correlation off Newfoundland, in the control region and where iceberg density is greatest (Fig. S2), but also other

273   patches of statistically significant positive and negative correlation elsewhere across the NW Atlantic (Fig. 5b).

274   However, many of these significant correlation patches, particularly south of 48°N, are linked to the variation in the

275   weather, as reflected in the NAO state 3 months previously (see Figs. 5c and d).

a) Correlation of local chl with the total number of icebergs on the main area

b) Same map with a 0.05 p-value sill

c) Correlation of local chl with the NAO index (3 months earlier)

d) Same map with a 0.05 p-value sill

e) Partial correlation of chl with icebergs, using NAO as control

f) Same map with a 0.05 p-value sill
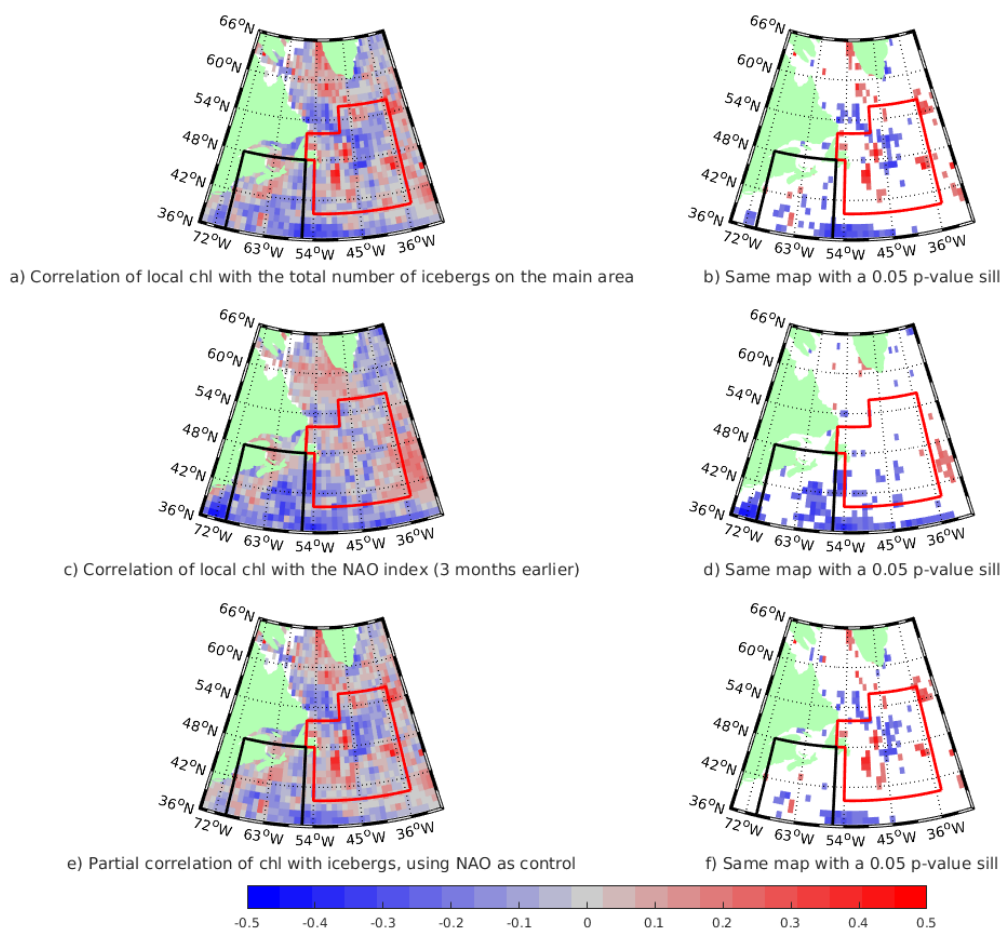
Figure 5: Correlation between local chlorophyll anomalies and 1) I_T, a) raw correlation; b) areas statistically significant at 0.05 level; 2) the NAO Index from 3 months earlier, c) raw correlation; d) areas statistically significant at 0.05 level; and 3) partial correlation with I_T, controlled by the NAO Index lagged by 3 months, e) raw correlation; f) areas statistically significant at 0.05 level. The main iceberg, and control, areas are shown in red and black respectively, as also shown in Figure 3.

The partial correlation, controlled for weather variability through use of the 3-month lagged NAO Index, is therefore shown in Figs. 5e and 5f. The latter shows that many of the more southerly statistically significant regions seen in Fig. 5b disappear under this control, however, the signal in the main area, off Newfoundland remains, as do areas off Greenland. These areas of statistically positive correlation that remain, however, tend to be somewhat fragmented and there are also some significant negative correlations in an arc from the Labrador coast into the central North Atlantic.

288   Nevertheless, note the lack of any coherent area of statistically significant partial correlation within the control region.

289   These equivocal signals are consistent with the limited direct correlation between I48N and chlorophyll shown in Fig. 4.

290   That analysis suggested that it required a month before the full impact of fertilization by the melting icebergs became

291   visible. The analysis is therefore extended to consider this lag component in more detail.

292   Using the technique outlined in Sect. 2.2.2, a series of partial correlations over 1998-2015 between 5 day series of I_T

293   and chlorophyll were carried out over a range of lags from 0 days to 70 days. A sub-set of the correlations showing

294   those squares with a statistical significant partial correlation at the 0.05 level is shown in Fig. 6. An animation of this

295   full correlation map sequence is available in the Supplementary Material. Note that the region over which correlations

296   are possible varies with the lag combination due to the persistent presence of cloud cover in the northern Atlantic

297   restricting the number of cloud-free pixels, particularly for the larger dataset of shorter lag.

298   This series of lagged partial correlations shows an interesting evolution, with a distinct zero lag positive correlation in

299   the vicinity of the main iceberg stream in the Labrador Current (that is, the main area of Fig. 3), changing towards a

300   more general, if lower, correlation over the NW Atlantic by a lag of 10 days, which then strengthens into a more

301   homogeneous region of positive correlation south of Greenland by day 20, peaking by day 30. This begins to decay

302   after day 30 and has essentially disappeared by day 50. There are initially some regions of relatively strong positive

303   correlation in the central east Atlantic and negative correlation in the control region and the Sargasso Sea, but these

304   decay fairly quickly. They are probably remnants of environmental chlorophyll impacts not due to the iceberg flux, but

305   not totally removed by the NAO control. A possible cause could be a light- and stratification-related spring bloom

306   signal (Behrenfeld and Boss, 2014) occurring during the peak iceberg months of April and May (Bigg et al., 2014). It is

307   also worth noting that the high chlorophyll correlation adjacent to the Greenland coast in Fig. 6 may be partially due to

308   local icebergs (not monitored by the IIP) or meltwater from Greenland glaciers (Arrigo et al., 2017). However these

309   local icebergs are closely confined to coastal waters (see charts at https://www.dmi.dk/en/groenland/hav/ice-charts/),

310   and the impact of local fjord meltwater is limited to periods after the I48N iceberg peak has decreased (early July

311   onwards) and restricted to the Greenland shelf region of the Labrador Sea (Arrigo et al., 2017). The majority of the

312   correlation signal south of 57°N is therefore likely due to the relationship with I48N rather than Greenland meltwater.

313

314
315
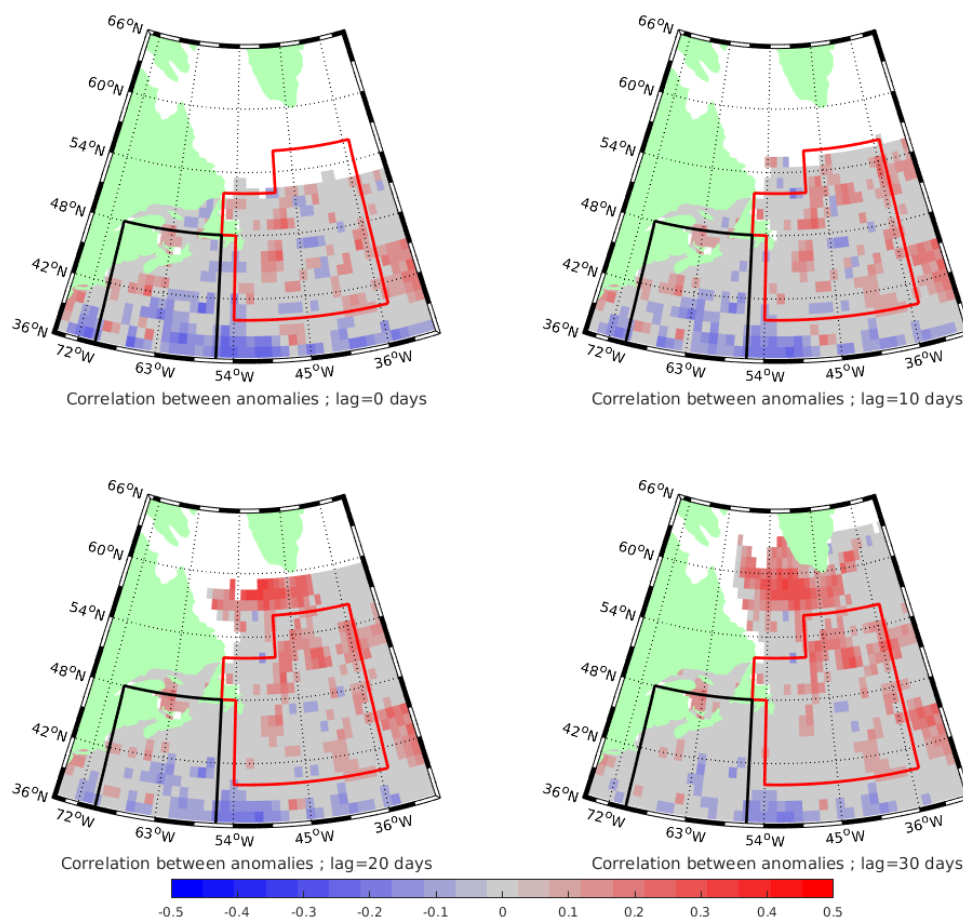
Figure 6: Partial correlation of I_T and chlorophyll at 4 different lags: a) 0 days; b) 10 days; c) 20 days; d) 30 days.
The gray shading area denotes where lag correlations for a particular lag are possible. The few correlations
outside [-0.5, 0.5] are set to the colour bar limit. The main iceberg, and control, areas are shown in red and black
respectively, as also shown in Figure 3.

4 Discussion

The approaches tested here for examining whether there is a measure of correlation between iceberg number density
and chlorophyll in the NW Atlantic all agree that one exists over the region, with the signal stronger with a lag of
several weeks to a month between a change in iceberg numbers and a response in the chlorophyll field. The NW
Atlantic, however, has distinctly different background conditions to the Southern Ocean, where both the size of the

326 icebergs and the high nutrient-low chlorophyll nature of the region allows clear and pronounced plumes of production

327 to be visibly associated with icebergs (Schwarz and Schodlok, 2009; Duprat et al., 2016; Wu and Hou, 2017). In the

328 NW Atlantic the peak of the natural light-driven spring bloom, enhanced by the inputs from land and coastal waters, as

329 well as the presence of a pronounced nutrient source through winter mixing (Fragoso et al., 2016), coincides with the

330 natural release of icebergs into the Labrador Current after being locked in winter sea-ice further north (Marko et al.,

331 1994). Thus, while a correlation between icebergs and chlorophyll is discernible in Figs. 4-6, the use of partial

332 correlations, with a control for chlorophyll in a control area (Fig. 4), and inter-annual and monthly climate variability

333 through the NAO (Figs. 5-6), was required to make the signal more robust.

334
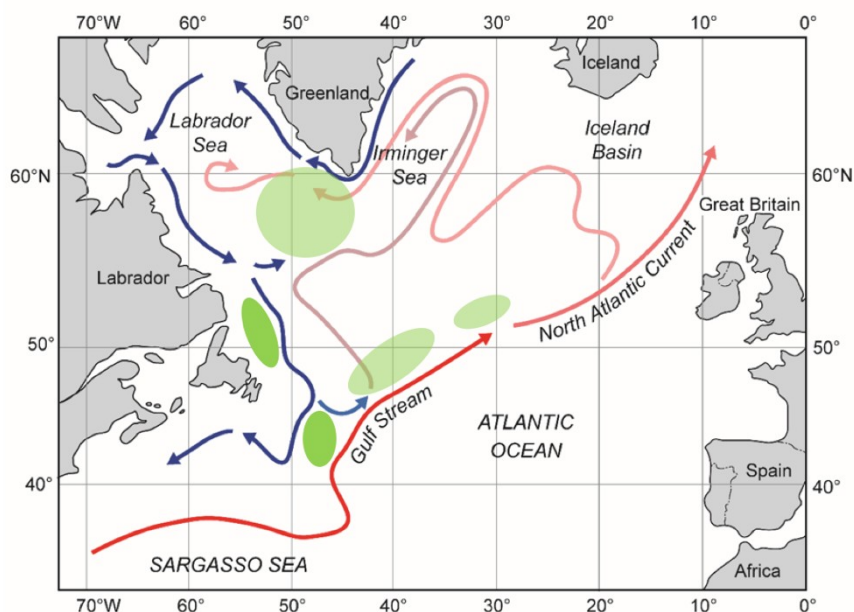
335 **Figure 7: A schematic of the surface circulation in the North Atlantic, derived from the satellite observations of**

336 **Ohashi et al. (2013). The colours are indicative of sea surface temperatures in the currents shown, varying from**

337 **cold (blue) to warm (red). The background shading schematically indicates proposed regions of iceberg**

338 **fertilization at lags of 0 (bright green) to 1 month (pale green), where the zero lagged fertilization is likely to be**

339 **due to the direct impact of the icebergs melting, while the delayed response is due to the impact of meltwater**

340 **advection. See text for more details. Note that the boundary of the Labrador Sea is taken to be the line extending**

341 **from the eastern tip of Newfoundland to the southern tip of Greenland.**

342

343   The lag of roughly a month between iceberg number increase and chlorophyll response, seen in Figs. 4 and 6, shows

344   that an indirect fertilization effect, following dispersing iceberg meltwater, is the most likely source for the delay. Figs.

345   5 and 6 both suggest an immediate, zero lag, impact of iceberg melting, but confined to the "Iceberg Alley" off the

346   coast of Newfoundland. However, Fig. 6 shows that the stronger lag relationship at 1 month seen in the main area

347   comparison of Fig. 4 is largely due to correlation in areas further east and north than the Labrador Current itself. This is

348   consistent with the iceberg meltwater and entrained nutrients from individual iceberg melting plumes (Smith et al.,

349   2013), with the resulting dispersion of accompanying fertilizing nutrients and trace elements from both types of sources,

350   being entrained into the North Atlantic Current and mixed into the Labrador Sea further east and north. A schematic of

351   this circulation and the associated iceberg fertilization is shown in Fig. 7. With a typical surface North Atlantic Drift

352   circulation, with a magnitude of ~ 0.5 ms^{-1} (Ohashi et al., 2013), in a month there is sufficient time for the dispersing

353   meltwater to travel ~ 1000 km, into the east of the Labrador Sea and the main North Atlantic Ocean, potentially leading

354   to the northward and eastward advective pattern shown in Fig. 6 and the Supplementary video. Note that the time delay

355   between melting and observed chlorophyll enhancement may be due to a number of causes and so difficult to confirm

356   without further modelling or observations. These causes, however, include i) direct effect of the meltwater dispersion,

357   ii) biologically-, chemically- or photoelectrically- induced delay in the conversion of iron from a colloidal to a

358   bioavailable form (Shaked and Lis, 2012; Raiswell et al., 2018), or iii) a time delay caused by the response of

359   phyotoplankton to the unevenly enriched environment.

360   Thus, the regional upper ocean circulation is consistent with the fertilization mechanism postulated by Smith et al.

361   (2013) for Greenland icebergs, and could underlie the partial correlation analyses shown here. Unfortunately, there are

362   no recorded direct observations of NW Atlantic individual icebergs showing clear fertilizing evidence. The NW

363   Atlantic, particularly in the spring, is a nutrient-rich area (Zhao et al., 2013; Saba et al., 2015). However, the region,

364   away from the vicinity of Greenland (Arrigo et al., 2017), is potentially subject to iron limitation (Rijkenberg et al.,

365   2014; Achterberg et al., 2018). While it cannot be definitively shown from observations at this time, it is possible that

366   the chlorophyll enhancement associated with higher iceberg density in the NW Atlantic is partially driven by the

367   dissolved iron supply (Raiswell et al., 2016; Raiswell et al., 2018) from the melting icebergs.

368   Nevertheless, it is possible to produce a first order estimate of the likely flux of iron delivered by icebergs to the NW

369   Atlantic. Raiswell et al. (2016) estimate net iceberg-derived Fe fluxes to the northern oceans of 0.7-5.5 Gmoles yr^{-1},

370   more than an order of magnitude greater than their estimated Fe atmospheric dust flux to the Arctic. While $\sim 80\%$ of the

371   former's iceberg Fe will be transported in icebergs calving from Greenland (Bigg et al., 1997), most such icebergs will

372   melt, either entirely or in large part, before they enter the Labrador Current. Marsh et al. (2018) estimated that only $\sim$

373   2.5% of the calved iceberg flux reaches the red box of the main area in Fig. 3. There is considerable calving variability

374   from year to year, resulting in wide variations in iceberg flux entering our core area from one year to the next (Bigg et

375   al., 2014), however, using Bamber et al.'s (2012) estimated mean 1958-2010 Greenland iceberg flux of 524±51 km^{3}yr^{-1}

376   leads to a mean iceberg flux of 13.1 km^{3}yr^{-1} entering our study area. This flux mostly melts over approximately the

377   three month period of April to June (Wilton et al., 2015). Using our above figures leads to a mean Fe flux to our core

378   area of 0.0047-0.0367 Gmoles/month. While icebergs are intrinsically isolated objects slowly melting over time during

379   their ocean passage, if we make the leading order approximation that the melt is spread roughly evenly over the ~

380   2.75x10^{12} m^2 of our core area, and noting 1 mole Fe ~ 0.056 kg, leads to a net iceberg-derived Fe flux to the core

381   Labrador Sea over the spring peak melt season of 9.57x10^{-8} -7.47x10^{-7} kgm^{-2}/month or 0.32- 2.49x10^{-8} kgm^{-2}d^{-1}.

382   This is a tiny Fe flux, subject to a wide range of uncertainty from a range of factors linked to the nature of icebergs

383   calved from Greenland, their survivability, and their passage through the Labrador Sea. However, it needs to be

384   compared to typical Fe fluxes to the surface Labrador Sea from other sources. Achterberg et al. (2018) estimated upper

385   ocean Fe fluxes in the sub-polar Atlantic from vertical upwelling to be much smaller than aerial fluxes, meaning this

386   component of Fe flux can be neglected. Shelley et al. (2017) measured dry and wet deposition aerial Fe fluxes from the

387   atmosphere to the ocean in spring 2014, the year of the greatest iceberg flux in the Labrador Current this century. They

388   found similar wet and dry deposition fluxes over the Labrador Sea of 1-2 µgm^{-2}d^{-1}, so giving a maximum of 4 µgm^{-2}d^{-1},

389   or 0.4x10^{-8} kgm^{-2}d^{-1}, of aerial Fe deposition. This value is similar to that at the minimum end of the above estimated

390   iceberg-delivered Fe flux during a normal year, let alone a year with roughly double the mean iceberg flux. This

391   suggests that in many years the iceberg-derived flux is likely to be a major Fe delivery mechanism to the Labrador Sea.

392

393   **5 Conclusion**

394   The analysis presented in this paper has shown that, if care is taken to minimize the impact of seasonal and weather-

395   related forcings, there is a weak but statistically significant correlation between iceberg number density and chlorophyll

396   concentrations approximately a month later in the NW Atlantic. This relationship is not so strongly spatially linked as in

397   the Southern Ocean (e.g. Duprat et al., 2016), and is found within an environment whose productivity is naturally highly

398   variable, even in the absence of icebergs (Fig. 1). However, the relationship was found in different approaches to

399   analysis of a mix of data sets. It is suggested that there is a physico-ecological relationship linked to the advection of

400   iceberg meltwater, both direct and from the impact of upwelling of basal meltwater plumes, and the nutrients and trace

401   elements the melt plume contains, leading to a small-scale local impact where icebergs are found off Newfoundland, but

402   a larger, delayed, impact downstream in the portion of the North Atlantic Drift entrained into the eastern Labrador Sea.

403   Smith et al. (2013) speculated that this iceberg effect was likely to exist in the North Atlantic and here we have moved

404   towards confirming its presence. The analysis has also shown that it is possible that it is iceberg-delivered Fe that

405   contributes to this enhanced productivity. In the Southern Ocean the impact of icebergs, and giant icebergs in particular,

406   on the storage of carbon in the deep ocean has been shown to be significant (Duprat et al., 2016). In the Northern

407   Hemisphere the difficulty of isolating the iceberg signal means this impact on the global carbon cycle is likely to be

408   much less here. However, the suggested enhancement of productivity by icebergs in the highly productive region of the

409   NW Atlantic means that this effect would be worth quantifying.

410

411   *Code and data availability.* Algorithms are available as Supplementary Material. All observational data used in this

412   study are available as described in section 2 Data.

413

414   *Author contributions.* QJ performed the analyses. GRB drafted the manuscript and led the project. RM contributed some

415   of the iceberg data and helped with the interpretation of the analysis. All authors contributed equally to the manuscript

416   beyond the initial draft.

417

418   *Acknowledgements.* We would like to thank ENSTA Paristech for giving QJ the opportunity to take a research

419   internship at the University of Sheffield during the summer preceding the fourth year of his Engineering degree (2017),

420   when the bulk of the research reported here was carried out. We are grateful to the US Coast Guard for compiling and

421   archiving IIP iceberg observations and charts, and to NASA for archiving the ocean colour datasets used here. Tom

422   Lees and Jacob Marsh assisted with digitization of the 2009-2015 IIP iceberg charts.

423

424   **APPENDIX A RECONSTRUCTING ICEBERG DENSITY USING MARKOV CHAINS**

425   The approach taken consists of running two algorithms, firstly one that builds the probability distribution of an iceberg

426   moving from one square to another in one day from a Markov chain, which is then used by a second algorithm that

427   constructs the iceberg density.

428   The first algorithm (Supplementary Algorithm 1) records every time an iceberg crosses from one grid square to another

429   in the form of a matrix, *Crossings*. In order to properly reflect the speeds of the icebergs the method also needs to

430   record all the times when the iceberg stayed in the same grid square - this corresponds to the diagonal of the matrix. So,

431   for example, if two sightings in two different squares are separated by N days, the algorithm assumes it spent one day

432   crossing the line and half of the remaining time ((N-1)/2) in each of the squares. Note that if between two sightings the

433   iceberg stayed in the same grid square, the algorithm counts N days as stationary. The final matrix of probabilities is a

434   normalized version of *Crossings*. There will be empty rows; these are rows that were never visited by icebergs. They

435   are completed by placing a 1 in the diagonal for mathematical convenience; this will have no impact on the simulations.

436   The second algorithm (Supplementary Algorithm 2) is the one that applies the Markov chain method. It only needs to

437   use the last known position of an iceberg before the 15th of the month and simulates its drifting for the remaining days.

438   To do this, it starts with a vector that has one iceberg in the index corresponding to the last known position, then it

439   multiplies this by the matrix of probabilities generated by Algorithm 1 to obtain the probabilities of presence for the

440   next day. This needs to be repeated for every remaining day until the 15th, which is equivalent to taking the matrix to

441   the power of the number of remaining days. Note that if the last sighting happens exactly on the 15th, then that power is

442   zero and the matrix reduces to the identity matrix, which will correctly record one iceberg at the right position. The

443   main caveat of this method is that it assumes that the probability of an iceberg crossing from one square to another is

444   independent of the time it spent in the former square. However, the procedure gave satisfactory results even with this

445   approximation.

References

Achterberg, E. P., Steigenberger, S., Marsay, C. M., LeMoigne, F. A. C., Painter, S. C., Baker, A. R., Connelly, D. P., Moore, C. M. *et al.* (2018) Iron biogeochemistry in the high latitude North Atlantic Ocean. *Sci. Rep.*, **8**, doi:
450   10.1038/s41598-018-19472-1.

Arrigo, K. R., van Dijken, G. L., Castelao, R. M., Luo, H., Rennermalm, Å. K., Tedesco, M., Mote, T. L., Oliver, H., and Yager, P. L. (2017) Melting glaciers stimulate large summer phytoplankton blooms in southwest Greenland waters, *Geophy. Res. Lett*., **44**, 6278-6285, 2017.

Bamber, J., van den Broecke, M., Ettema, J., Lenaerts, J., and Rignot, E. (2012) Recent large increases in freshwater fluxes
455   from Greenland into the North Atlantic. *Geophys. Res. Lett.,* **39**, L19501.

Behrenfeld, M. J., and Boss, E. S. (2014). Resurrecting the ecological underpinnings of ocean plankton blooms. *Ann. Rev. Mar. Sci.*, **6**, 167-194.

Bhatia, M. P., Kujawinski E. B., Das S. B., Breier, C. F., Henderson, P. B., and Charette, M. A. (2013) Greenland meltwater as a significant and potentially bioavailable source of iron to the ocean. *Nature Geosci.*, **6**, 274–278.

460   Biddle, L. C., Kaiser, J., Heywood, K. J., Thompson, A. F., and Jenkins, A. (2015) Ocean glider observations of iceberg-enhanced biological production in the northwestern Weddell Sea. *Geophys. Res. Lett.,* **42**, 459-465.

Bigg, G. R., Wadley, M. R., Stevens, D. P., and Johnson, J. A. (1997) Modelling the dynamics and thermodynamics of icebergs. *Cold Regions Sci. Technol.,* **26**, 113-135.

Bigg, G. R., Wei, H., Wilton, D. J., Zhao, Y., Billings, S. A., Hanna, E., and Kadirkamanathan, V. (2014) A century of
465   variation in the dependence of Greenland iceberg calving on ice sheet surface mass balance and regional climate change. *Proc. Roy. Soc. Ser. A,* **470**, 20130662, doi:10.1098/rspa.2013.0662.

Christensen, E., and Luzader, J. (2012) From sea to air to space: a century of iceberg tracking technology. *Coast Guard Proc. Mar. Safety Security Council,* **69**, 17-22.

Djavidnia, S., Melin, F., and Hoepffner, N. (2010) Comparison of global ocean colour data records. *Ocean Sci.,* **6**, 61-76.

470   Duprat, L. P. A. M., Bigg, G. R., and Wilton, D. J. (2016) Enhanced Southern Ocean marine productivity due to fertilization by giant icebergs. *Nature Geosci.*, **9**, 219-221.

Ferrara, M., Groff, F., Keshavamurthy, K., Robeson, S. M., and Kieu, C. (2017) Large-scale control of the lower stratosphere on variability of tropical cyclone intensity. *Geophys. Res. Lett.*, **44**, 4313-4323.

Fragoso, G. M., Poulton, A. J., Yashayaev, I., Head, E. J. H., Stinchcombe, M. C., Purdie, D. A. (2016) Biogeographical
475   patterns and environmental controls of phytoplankton communities from contrasting hydrographic zones of the Labrador Sea. *Prog. Oceanogr.,* **141**, 212-226.

Hanna, E., Huybrechts, P., Cappelen, J., Steffen, K., Bales, R. C., Burgess, E., McConnell, J., Steffensen, J. P., Van den Broeke, M., Wake, L., Bigg, G. R., Griffiths, M., and Savas, D.: Greenland Ice Sheet surface mass balance 1870 to 2010 based on Twentieth Century Reanalysis, and links with global climate forcing, J. Geophys. Res. Atmos., 116, D24121, doi:10.1029/2011JD016387, 2011.

Hawkings, J. R., Wadham, J. L., Tranter, M., Raiswell, R., Benning, L. G., Statham, P. J., Tedstone, A., Nienow, P. *et al.* (2014) Ice sheets as a significant source of highly reactive nanoparticulate iron to the oceans. *Nat. Commun.*, **5**, doi: 10.1038/ncomms4929.

Harrison, W. G., and Li, W. K. W. (2008) Phytoplankton growth and regulation in the Labrador Sea: light and nutrient limitation. *J. Northwest Atl. Fish. Sci.*, **39**, 71–82.

He, Z., Wu, R., and Wang, W. (2016) Signals of the South China Sea summer rainfall variability in the Indian Ocean. *Clim. Dyn.*, **46**, 3181-3195.

Helly, J. J., Kaufmann, R. S., Stephenson, G. R., and Vernet, M. (2011) Cooling, dilution and mixing of ocean water by free-drifting icebergs in the Weddell Sea. *Deep-Sea Res. II,* **58**, 1336-1345.

Hendry, K. R., Huvenne, V. A. I., Robinson, L. F., Annett, A., Badger, M., Jacobel, A. W., Ng, H. C., Opher, J. *et al.* (2019) The biogeochemical impact of glacial meltwater from southwest Greenland. *Prog. Oceanogr.*, **176**, doi:10.1016/j.pocean.2019.102126.

Holmquist, C. (1958) An observation on young specimens of *Ammodytes dubius*. *Meddelelser Grønl.,* **159**, 1–14.

Hong, C.-C., Lee, M.-Y., Hsu, H.-H., and Tseng, W.-L. (2018) Distinct influences of the ENSO-like and PMM-like SS anomalies on the mean TC genesis location in the western North Pacific: the 2015 summer as an extreme example. *J. Clim.*, **31**, 3049-3059.

Hopwood, M. J., Bacon, S., Arendt, K., Connelly, D. P. and Statham, P. J. (2015) Glacial meltwater from Greenland is not likely to be an important source of Fe to the North Atlantic. *Biogeochem.*, **124**, 1-11.

Hopwood, M. J., Carroll, D., Browning, T. J., Meire, L., Mortensen, J., Krisch, S., and Achterberg, E. P.: Non-linear response of summer-time marine productivity to increased meltwater discharge around Greenland, Nature Comm., 9, https://doi.org/10.1038/s41467-018-05488-08, 2018.

Hopwood, M. J., Carroll, D., Höffer, J., Achterberg, E. P., Meire, L., Le Moigne, F. A. C., Bach, L. T., Eich, C., Sutherland, D. A., and González, H. E.: Highly variable iron content modulates iceberg-ocean fertilisation and potential carbon export, Nature Comm., 10, 5261, https://doi.org/10.1038/s41467-019-13231-0, 2019.

Hurrell, J. W, and Deser, C. (2009) North Atlantic climate variability: The role of the North Atlantic Oscillation. J. *Mar. Sys*., **78**, 28-41.

International Ice Patrol (1995), updated 2016. *International Ice Patrol (IIP) Iceberg Sightings Database, Version 1*. Boulder, Colorado USA. NSIDC: National Snow and Ice Data Center. doi: http://dx.doi.org/10.7265/N56Q1V5R. [Date Accessed: 4 January 2018].

510   Joiris, C. R. (2018) Hotspots of kittiwakes Rissa tridactyla tridactyla on icebergs off southwest Greenland in autumn. *Pol. Biol.,* **11**, 2375-2378.

Lancelot, C., de Montety, A., Goosse, H., Becquevort, S., Schoemann, V., Pasquer, B., and Vancoppenolle, M. (2009) Spatial distribution of the iron supply to phytoplankton in the Southern Ocean: a model study. *Biogeosci.*, **6**, 2861-2878.

Marko, S. R., Fissel, D. B., Wadhams, P., Kelly, P. M., and Brown, R. D. (1994) Iceberg severity off eastern North America

515   – its relationship to sea-ice variability and climate-change. *J. Clim*., **7**, 1335-1351.

Marsh, R., Bigg, G. R., Zhao, Y., Martin, M. J., Blundell, J. R., Josey, S. A., Hanna, E., and Ivchenko, V. (2018) Prospects for seasonal forecasting of iceberg distributions in the North Atlantic. *Nat. Hazards,* **91**, 447-471.

Martin, P., van der Loeff, M. R., Cassar, N., Vandromme, P., d'Ovidio, F., Stemmann, L., Rengarajan. R., Soares, M. *et al.* (2013) Iron fertilization enhanced net community production but not downward particle flux during the Southern Ocean

520   iron fertilization experiment, LOHAFEX. *Glob. Biogeochem. Cyc.,* **27**, 871-881.

Morita, K., and Fukuwaka, M. (2020) Intra- and interspecific density-dependent growth and maturation of Pacific salmon in the Bering Sea. *Ecol. Res.*, **35**, 106-112.

Ohashi, K., Han, G., Chen, N., and Helbig, J. (2013) Northwest Atlantic surface circulation from multi-satellite observations. *J. Atmos.-Ocean*, **51**, 35-49.

525   Perner, K., Moros, M., Otterå, O. H., Blanz, T., Schneider, R. R., and Jansen, E. (2019) An oceanic perspective on Greenland's recent freshwater discharge since 1850. *Sci. Rep.*, **9**, doi:10.1038/s41598-019-53723-z.

Raiswell, R. Benning, L. G., Tranter, M., and Tulaczyk, S. (2008) Bioavailable iron in the Southern Ocean: the significance of the iceberg conveyor belt. *Geochem. Trans.*, **9**, doi: 10.1186/1467-4866-9-7.

Raiswell, R., Hawkings, J. R., Benning, L. G., Baker, A. R., Death, R., Albani, S., Mahowald, N., Krom, M. D. *et al.* (2016)

530   Potential bioavailable iron delivery by iceberg-hosted sediments and atmospheric dust to the polar oceans. *Biogeosci.,* **13**, 3887-3900.

Raiswell, R., Hawkings, J., Elsenousy, A., Death, R., Tranter, M., and Wadham, J. (2018) Iron in glacial systems: speciation, reactivity, freezing behaviour, and alteration during transport. *Front. Earth Sci.*, **6**, 222, doi:10.3389/feart.2018.00222.

Reintges, A., Latif, M., and Park, W.: Sub-decadal North Atlantic Oscillation variability in observations and the Kiel climate

535   model, Clim. Dyn., 48, 3475-3487, doi: 10.1007/s00382-016-3279-0, 2017.

Rijkenberg, M. J. A., Middag, R., Laan, P., Gerringa, L. J. A., van Aken, H. M., Schoemann, V., de Jong, J. T. M., and de Baar, H. J. W. (2014) The distribution of dissolved iron in the west Atlantic Ocean. *PLOS One,* **9**, doi:10.1371/journal.pone.0101323.

Saba, V. S., Hyde, K. J. W., and Rebuck, N. D. (2015) Physical associations to spring phytoplankton biomass interannual

540   variability in the US Northeast Continental Shelf. *J. Geophys. Res. Biogeosci.*, **120**, 205-220.

Schwarz, J. N., and Schodlok, M. P. (2009) Impact of drifting icebergs on surface phytoplankton biomass in the Southern Ocean: ocean colour remote sensing and in situ iceberg tracking. *Deep-Sea Res. I*, **56**, 1727-1741.

Shaked, Y., and Lis, H. (2012) Disassembling iron availability to phytoplankton. *Fron. Microbiol.*, **3**, doi:10.3389/fmicb.2012.00123.

545 Shaw, T. J., Raiswell, R., Hexel, C. R., Vu, H. P., Moore, W. S., Dudgeon, R., and Smith Jr., K. L. (2011) Input, composition and potential impact of terrigenous material from free-drifting icebergs. *Deep-Sea Res. II*, **58**, 1376-83.

Shelley, R. U., Roca-Martí, M., Castrillejo, M., Sanial, V., Masqué, P., Landing, W. M., van Beek, P., Planquette, H., *et al.* (2017) Quantification of trace element atmospheric deposition fluxes to the Atlantic Ocean (> 40ᵒN; GEOVIDE, GEOTRACES GA01) during spring 2014. *Deep-Sea Res. I,* **119**, 34-49.

550 Shulenberger, E. (1983) Water-column studies near a melting Arctic iceberg. *Polar Biol.,* **2**, 149–158.

Smith Jr., K. L., Robison, B. H., Helly, J. J., Kaufmann, R. S., Ruhl, H. A., Shaw, T. J., Twining, B. S., and Verrnet, M. (2007) Free-drifting icebergs: hot spots of chemical and biological enrichment in the Weddell Sea. *Science*, **317**, 478-82.

Smith Jr., K. L., Sherman, A. D., Shaw, T. J., Murray, A. E., Vernet, M., and Cefarelli, A. O. (2011) Carbon export associated with free-drifting icebergs in the Southern Ocean. *Deep-Sea Res. II*, **58**, 1485-1496.

555 Smith Jr., K. L., Sherman, A. D., Shaw, T. J., and Sprintall, J. (2013) Icebergs as unique Lagrangian ecosystems in polar seas. *Ann. Rev. Mar. Sci.,* **5**, 269-287.

Srinivas, G., Chowdary, J. S., Kosaka, Y., Gnanaseelan, C., Parekh, A., and Prasad, K. V. S. R. (2018) Influence of the Pacific-Japan Pattern on Indian Summer Monsoon rainfall. *J. Clim.*, **1**, 3943-3958.

Statham, P. J., Skidmore, M., and Tranter, M. (2008) Inputs of glacially derived dissolved and colloidal iron to the coastal
560 ocean and implications for primary productivity. *Glob. Biogeochem. Cyc.* **22**, doi: 10.1029/2007GB003106.

Stuart, A., Ord, J. K., and Arnold, S. (2008) Kendall's Advanced Theory of Statistics, Volume 2A, Classical Inference and the Linear Model, 6ᵗʰ ed., Wiley, Chichester.

Vorosmarty, C. J., Fekete, B. M., and Tucker, B. A. (1998) Global river discharge, 1807-1991, V1.1 (RivDIS). Dataset. Available online [http://www.daac.ornl.gov] from Oak Ridge National Laboratory Distributed Active Archive Center,
565 Oak Ridge, Tennessee, U.S.A.

Wadley, M. R., Jickells, T. D., and Heywood, K. J. (2014) The role of iron sources and transport for Southern Ocean productivity. *Deep-Sea Res. I*, **87**, 82-94.

Wang, S., Yeager, K. M., and Lu, W. (2016) Carbon isotope fractionation in phytoplankton as a potential proxy for pH rather than for [CO_2(aq)]: observations from a carbonate lake. *Limnol. Oceanogr.*, **61**, 1259-1270.

570 Wilton, D. J., Bigg, G. R., and Hanna, E. (2015) Modelling twentieth century global ocean circulation and iceberg flux at 48ᵒN: implications for west Greenland iceberg discharge. *Prog. Oceanogr.,* **138**, 194-210.

Wu, S. Y., and Hou, S. (2017) Impact of icebergs on net primary productivity in the Southern Ocean. *Cryosphere*, **11**, 707-722.

Yang, Y., Russell, L. M., Lou, S., Liu, Y., Singh, B., and Ghan, S. J. (2016) Rain-aerosol relationships influenced by wind
575 speed. *Geophys. Res. Lett.*, **43**, 2267-2274.

Yankovsky, A. E., and Yashayaev, I. (2014) Surface buoyant plumes from melting icebergs in the Labrador Sea. *Deep-Sea Res. I,* **91**, 1-9.

Zhao, H., Han G., and Wang, D. (2013) Timing and magnitude of spring bloom and effects of physical environments over the Grand Banks of Newfoundland. *J. Geophys. Res. Biogeosci.*, **118**, 1385-1396.

580   Zhao, Y., Bigg, G. R., Billings, S. A., Hanna, E., Sole, A. J., Wei, H., Kadirkamanathan, V., and Wilton, D. J.: Inferring the variation of climatic and glaciological contributions to West Greenland iceberg discharge in the Twentieth Century, *Cold Reg. Sci. Technol.*, 121, 167-178**,** doi:10.1016/j.coldregions.2015.08.006, 2016.